applied optics

Active alignment of complex perturbed pupil-offset off-axis telescopes using the extension of nodal aberration theory

Ming Wen,[1,2] Hongcai Ma,[1,*] and Chengshan Han[1]

[1]Changchun Institute of Optics, Fine Mechanics and Physics, Chinese Academy of Sciences, Changchun 130033, China
[2]University of Chinese Academy of Sciences, Beijing 100049, China
*Corresponding author: mahc@ciomp.ac.cn

Received 5 February 2021; revised 11 April 2021; accepted 11 April 2021; posted 12 April 2021 (Doc. ID 421611); published 27 April 2021

This paper presents an optical alignment strategy for complex perturbed pupil-offset off-axis reflective telescopes, based on the extension of nodal aberration theory (NAT). First, the direct expansion of the wave aberration function in the vector form for perturbed off-axis systems is given, which is especially convenient for the expansion of the corresponding higher-order terms. The inherent vector relationships between the contributions generated by the aberrations of the on-axis parent systems through pupil transformation are disclosed in detail, which is helpful to understand the aberration behavior of off-axis systems. Then, according to the inherent vector relationships, an analytical alignment model based on NAT for complex cases of perturbed off-axis telescopes is established. It can quantitatively separate the effects of misalignments and surface figure errors from the total aberration fields. The alignment model is solved by using particle swarm optimization algorithm. Then, an optical alignment example of the off-axis three-mirror anastigmatic telescope with misalignments and complex surface figure errors based on the proposed method is demonstrated. After correction, the perturbed telescope can be nearly restored to the nominal states. Finally, Monte Carlo simulations are carried out to show the effectiveness and accuracy of the proposed method.

https://doi.org/10.1364/AO.421611

1. INTRODUCTION

Compared with refractive optical telescopes, reflective optical telescopes have the advantages of high transmission, wide spectrum, radiation resistance, no chromatic aberrations, and so on. Due to the weight limitation of space-based systems, the mirrors and supporting structures will have to be lightweight. This kind of system is easily affected by severe environments such as thermal stress and vibration, which will degrade the imaging capabilities. Because of the increase of the aperture size and performance requirements, it is necessary to equipped it with the active optics system [1–5] to correct the component perturbations (component misalignments or surface deformations). In on-axis reflective telescopes, the spider and the mirror obscuration limit the energy concentration, signal-to-noise ratio and field-of-view (FOV), and so on. To overcome these shortcomings, off-axis reflective telescopes have been developed [6,7]. However, the rotational symmetry of off-axis telescopes is broken, and the aberration field characteristics become more complex. Thus, the alignment or active alignment of off-axis telescopes becomes more challenging.

To correct the perturbed telescopes, it is necessary to quantitatively determine the perturbation values. To determine these perturbation values, some methods were presented, which are sensitivity table (ST) method, reverse optimization (RO) method, the method based on nodal aberration theory (NAT), and so on. Among them, the ST method [8] is commonly used. Because this method basically adopts linear approximation, the accuracy is limited by the assumption. As the perturbation ranges increase, the linear relationship will be broken, and the calculated perturbation values using the sensitivity table may be inaccurate. Moreover, in some optical systems, perturbation parameters are likely to be strongly coupled, which can lead to the singularity problem in the ST method, and the calculated perturbation values can also be inaccurate. The RO method [9] uses the optimization module of optical design software to obtain the perturbation values, which is difficult to implement on orbit. Moreover, most of these methods are numerical, which can hardly provide deep theoretical guidance for system alignment, and there exist some problems in practical application. To overcome these shortcomings, the method based on NAT is proposed.

NAT is a very powerful tool for design, analysis, and alignment of nonsymmetrical optical systems, which was discovered by Shack [10] and developed by Thompson [11–15]. The current research on the alignment of off-axis and on-axis telescopes using nodal aberration theory can be mainly categorized

into two groups: one to discuss the aberration field characteristics, and the other to discuss the calculation of perturbation parameters. For the first group, the focus is on discussing the characteristics of aberration fields in the presence of different kinds of misalignments or other perturbations based on nodal aberration theory, and also the relationships between several derived aberrations [16–19]. For the second group, the calculation of perturbation parameters based on nodal aberration theory is mainly discussed [20–24]. In the second group, an optical compensation method for the perturbed three mirror anastigmatic telescopes based on NAT was presented [20], which mainly discussed the corresponding compensation strategy. An optical alignment method for off-axis telescopes based on NAT was reported [21], which mainly separated the specific aberration contributions of lower-order aberrations (astigmatism and coma) from the total aberrations, and the aberration relationships of the off-axis systems with decentered pupil center on y-axis were given. These methods mainly focus on some simple cases of perturbed telescopes, which only involve some lower-order aberrations and simple surface figure errors. For these simple cases, they are effective. However, for complex cases of off-axis telescopes (e.g., with complex surface figure errors, freeform surfaces, or large FOV), the contributions of higher-order aberrations should be considered, which can improve the alignment accuracy and shorten the alignment period. As far as we know, the analytical optical alignment method involving higher-order aberrations for off-axis telescopes has been rarely reported. Therefore, this paper proposes an alignment strategy involving higher-order aberrations for complex perturbed off-axis telescopes based on the extension of NAT, which uses the inherent vector relationships between the derived aberrations of off-axis telescopes.

This paper is organized as follows. In Section 2, the general vector expansion of wave aberration function and the inherent relationships between the derived aberration contributions for perturbed off-axis systems are presented. Section 3 provides an alignment strategy for complex cases of off-axis telescopes based on these inherent relationships. Verification of system alignment for the perturbed off-axis three-mirror anastigmatic (TMA) telescope with misalignments and complex figure errors (including Zernike astigmatism, trefoil, and tetrafoil) are illustrated in Section 4. The paper is concluded in Section 5.

2. GENERAL VECTOR EXPANSION OF WAVE ABERRATION FUNCTION AND INHERENT VECTOR RELATIONSHIPS FOR PERTURBED OFF-AXIS TELESCOPES

A. General Expansion of Wave Aberration Function in the Vector Form for Perturbed Off-Axis Systems

The wave aberration in an optical system consists of all-surface contributions. The vector form of wave aberration function in rotationally symmetric systems is expressed as [11]

$$W=\sum_{j}\sum_{p}^{\infty}\sum_{n}^{\infty}\sum_{m}^{\infty}(W_{klm})_j(\vec{H}\cdot\vec{H})^p(\vec{\rho}\cdot\vec{\rho})^n(\vec{H}\cdot\vec{\rho})^m, \tag{1}$$

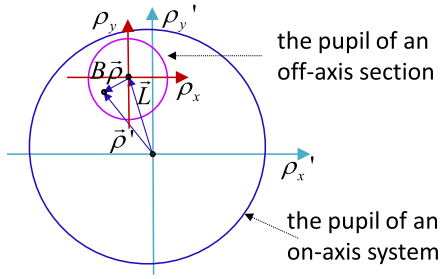

Fig. 1. Representation of the relationship between the parent pupil and the decentered pupil vector.

where $k=2p+m$ and $l=2n+m$, $\vec{H}$ denotes the normalized field vector, $\vec{\rho}$ designates the normalized pupil vector, and $(W_{klm})_j$ denotes the corresponding aberration coefficient.

The off-axis system in this paper refers to the pupil-offset off-axis system, which can be considered to be an off-axis portion of a rotationally symmetric on-axis system. The transformation relationship between the parent pupil vector and the decentered pupil vector is shown in Fig. 1, which can be expressed by

$$\vec{\rho}'=B\vec{\rho}+\vec{L}, \tag{2}$$

where B denotes the scaling factor, and $\vec{L}$ designates the pupil decenter vector normalized by the pupil radius of the parent system. Furthermore, $\vec{\rho}'$ and $\vec{\rho}$ denote the normalized pupil vectors of the parent system and the decentered system, respectively.

The aberration properties of pupil decentered optical systems without misalignment were described in [25,26]. To develop a mathematical expression of the aberration field for a misaligned system, an effective field vector was introduced [27]. The effective field vector for the jth surface is written as

$$\vec{H}_{Aj}=\vec{H}-\vec{\sigma}_j, \tag{3}$$

where $\vec{\sigma}_j$ denotes the aberration field decenter vector for surface j, which is directly related to the corresponding misalignment parameters.

In the presence of misalignment, the wave aberration function in off-axis optical systems in vector form can be expressed by

$$W=\sum_{j}\sum_{p}^{\infty}\sum_{n}^{\infty}\sum_{m}^{\infty}(W_{klm})_j(\vec{H}_{Aj}\cdot\vec{H}_{Aj})^p \times[(B\vec{\rho}+\vec{L})\cdot(B\vec{\rho}+\vec{L})]^n[\vec{H}_{Aj}\cdot(B\vec{\rho}+\vec{L})]^m. \tag{4}$$

To facilitate the following discussion, the field and pupil dependence of each term in Eq. (4) can be explicitly expressed based on the rules of vector multiplication. In the derivation of the following several equations, Eq. (2) and Eq. (3) in Ref. [16] are used. The difference is that the corresponding variables are different, and the variable substitution is needed. Here, we will make a further discussion, which is more convenient and direct to get the explicit expansion of the aberration function in off-axis systems. The wave aberration function, in Eq. (4), can be rewritten as

$$W=\sum_{j}\sum_{p}^{\infty}\sum_{n}^{\infty}\sum_{m}^{\infty}\vec{U}(\vec{H}_{Aj})\cdot\vec{T}(\vec{\rho}), \tag{5}$$

where

$$\vec{U}(\vec{H}_{Aj}) = W'_{klmj}[(\vec{H}_{Aj}\cdot\vec{H}_{Aj})^p(\vec{H}_{Aj})^m]$$
$$\vec{T}(\vec{\rho}) = [(B\vec{\rho}+\vec{L})\cdot(B\vec{\rho}+\vec{L})]^n(B\vec{\rho}+\vec{L})^m$$
$$W'_{klm} = \sum_{t=0}^{s}\frac{1}{2^{m+2t-1+\delta_{m0}}}\binom{m+2t}{t}W_{kl(m+2t)},$$
$$s = \min\{n,\ p\}, \tag{6}$$

and where $\vec{U}(\vec{H}_{Aj})$ denotes the terms corresponding to the effective field vector, $\vec{T}(\vec{\rho})$ denotes the terms corresponding to the pupil vector, and $\delta_{m,0}$ is the Kronecker delta function ($\delta_{m,0}=0$ if $m\neq 0$; $\delta_{m,0}=1$ if $m=0$). Equation (5) is the aberration function for the misaligned off-axis systems, which can analytically describe how the aberration fields of the off-axis systems change with the pupil coordinate, field coordinate, as well as misalignments. As can be seen, the field and pupil dependence have been explicitly separated. The coefficients in Eq. (4) are different from those in Eq. (5), and their relationships have been given. The contributions of the intrinsic and extrinsic aberrations are considered in the aberration coefficients.

Using the binomial theorem, the pupil dependence of each term can be expanded. In Eq. (5), each term can be rewritten as

$$\begin{aligned}
&\vec{U}\cdot(B\vec{\rho}+\vec{L})^m[(B\vec{\rho}+\vec{L})\cdot(B\vec{\rho}+\vec{L})]^n\\
&=\left[\sum_{f=0}^{m}\binom{m}{f}B^f\vec{U}\cdot\vec{L}^{m-f}\vec{\rho}^f\right]\\
&\times\left[\sum_{g=0}^{n}\binom{n}{g}[2B(\vec{\rho}\cdot\vec{L})+(\vec{L}\cdot\vec{L})]^{n-g}[B^2(\vec{\rho}\cdot\vec{\rho})]^g\right]\\
&=\left[\sum_{f=0}^{m}\binom{m}{f}B^f\vec{U}\cdot\vec{L}^{m-f}\vec{\rho}^f\right]\\
&\times\left[\sum_{g=0}^{n}\sum_{h=0}^{n-g}\binom{n}{g}\binom{n-g}{h}2^hB^{2g+h}(\vec{L}\cdot\vec{L})^{n-g-h}(\vec{\rho}\cdot\vec{L})^h(\vec{\rho}\cdot\vec{\rho})^g\right]\\
&=\sum_{f=0}^{m}\sum_{g=0}^{n}\sum_{h=0}^{n-g}\xi_{fgh}\left[(\vec{L}^*)^{m-f}\vec{L}^h(\vec{L}\cdot\vec{L})^{n-g-h}\vec{U}\right.\\
&\left.\cdot\vec{\rho}^{f+h}(\vec{\rho}\cdot\vec{\rho})^g+(\vec{L}\cdot\vec{L})^{n-g-h}(\vec{V}\cdot\vec{\rho}^{|f-h|})(\vec{\rho}\cdot\vec{\rho})^{r+g}\right],
\end{aligned}\tag{7}$$

where

$$\xi_{fgh} = \sum_{t=0}^{q}\frac{1}{2^{\delta_{h0}}}\binom{h+2t}{t}\binom{m}{f}\binom{n}{g-t}\times\binom{n-(g-t)}{h+2t}B^{f+2g+h},\ q=\min\{g,\ (n-g-h)\}$$
$$\vec{V} = \begin{cases}(\vec{L}^{m-f+h})^*\vec{U}, & f\geq h\\ \vec{L}^{m-f+h}\vec{U}^*, & f<h\end{cases}$$
$$r = \min\{f,\ h\}. \tag{8}$$

The asterisk superscript represents the conjugate of the corresponding vector. According to Eq. (7), the aberration terms in Eq. (5) can be converted into existing aberration types.

By using the similar method, the expansion of the field dependence of each term in Eq. (5) can also be obtained. It is especially convenient for the expansion of high-order terms of wave aberration function in off-axis systems. Based on the general formula, the wave aberration expansion through fifth order and partial seventh order, as examples, will be given in the following.

B. Inherent Relationships between the Aberration Contributions Generated through Pupil Transformation for Perturbed Off-Axis Systems

The Zernike polynomials are particularly attractive in wavefront analysis because of the orthogonality over the unit circle. There are several definitions of the Zernike polynomials. Here, the Fringe Zernike polynomials [28] are used, which employ amplitude normalization. To make Zernike description related to the NAT expression, the wave aberration function can also be expanded over the Zernike polynomial vectors, which is given by

$$W(\vec{\rho}) = \sum_{n'=0}^{\infty}\sum_{m'=0}^{n'}\vec{C}_{n'm'}\cdot\vec{Z}_{n'}^{m'}(\vec{\rho}). \tag{9}$$

Here, $\vec{Z}_{n'}^{m'}(\vec{\rho})$ denotes the Fringe Zernike vector, which can be expressed as

$$\vec{Z}_{n'}^{m'}(\vec{\rho}) = \sum_{s=0}^{(n'-m')/2}\frac{(-1)^s(n'-s)!}{s!(\frac{n'+m'}{2}-s)!(\frac{n'-m'}{2}-s)!}(\vec{\rho}\cdot\vec{\rho})^{\frac{n'-m'-2s}{2}}\vec{\rho}^{m'}, \tag{10}$$

where $\vec{C}_{n'm'}$ denotes the corresponding Fringe Zernike coefficient vector, and n' and m' are positive integers (including zero) known as the radial degree and the azimuthal frequency, respectively. It should be noted that $n'-m'\geq 0$ and $n'-m'$ must be an even number.

In a rotationally symmetric system, the relationships between the Seidel aberrations and the Fringe Zernike aberrations are relatively simple. However, in perturbed off-axis systems, the relationships between them are complex due to the influence of pupil coordinate transformation. In particular, the aberrations with higher-order pupil dependence will generate some lower-order aberrations through pupil transformation. According to Eq. (7), the aberration expansion including higher-order terms for perturbed off-axis systems can be obtained. Then, according to Eq. (10), all the aberrations can be rewritten to the form of Eq. (9). The contributions generated by the aberrations of the on-axis parent systems through pupil transformation to Zernike polynomial vectors are shown in Table 1 (expanded through seventh order). The first column in Table 1 shows the aberration types of the on-axis parent systems. The subscript M indicates that the corresponding aberrations are obtained with reference to the medial focal surface. The first row in Table 1, the notations ($\vec{Z}_2^2$, $\vec{Z}_3^1$, etc.), denote the corresponding Zernike polynomial vectors. Among them, $\vec{Z}_4^0$, $\vec{Z}_6^0$, and $\vec{Z}_8^0$ are scalars, not vectors, but scalars can also be considered a special form of vectors, which are the useful extension to unified vector description. In Table 1, the black square indicates that there is the contribution to the corresponding Zernike vector. Here,

Table 1. Contributions Generated by the Aberrations of the On-Axis Parent Systems through Pupil Transformation to Zernike Polynomial Vectors

Aberration Type	$\vec{Z}_2^2$	$\vec{Z}_3^1$	$\vec{Z}_4^0$	$\vec{Z}_3^3$	$\vec{Z}_4^2$	$\vec{Z}_5^1$	$\vec{Z}_6^0$	$\vec{Z}_4^4$	$\vec{Z}_5^3$	$\vec{Z}_6^2$	$\vec{Z}_7^1$	$\vec{Z}_8^0$
W_{131}	■	■										
W_{222}	■											
W_{040}	■	■	■									
W_{331M}	■	■										
W_{422}	■											
W_{333}	■			■								
W_{240M}	■	■	■									
W_{242}	■	■		■	■							
W_{151}	■	■	■	■	■	■						
W_{060}	■	■	■	■	■	■	■					
W_{531M}	■	■										
W_{622}	■											
W_{444}	■			■				■				
W_{440M}	■	■	■									
W_{533}	■			■								
W_{260M}	■	■	■	■	■	■	■					
W_{442M}	■	■		■	■							
W_{351M}	■	■	■	■	■	■						
W_{353}	■	■		■	■			■	■			
W_{171}	■	■	■	■	■	■	■	■	■	■	■	
W_{262}	■	■	■	■	■	■		■	■	■		
W_{080}	■	■	■	■	■	■	■	■	■	■	■	■

in accordance with the tradition of optical testing, the x-axis is chosen as the reference axis [29], and the angle is measured counterclockwise.

Table 1 implies that the third-order coma of the on-axis parent systems will make the contributions to Zernike coma ($\vec{Z}_3^1$) and Zernike astigmatism ($\vec{Z}_2^2$); the third-order spherical aberration will make the contributions to Zernike astigmatism, Zernike coma, and Zernike spherical aberration ($\vec{Z}_4^0$); the derived contributions of tetrafoil of the on-axis parent systems include Zernike astigmatism, Zernike trefoil ($\vec{Z}_3^3$), and Zernike tetrafoil ($\vec{Z}_4^4$); and the derived contributions of the seventh-order spherical aberration include all the lower-order Zernike aberrations. Almost all aberrations of the on-axis parent systems have derived contributions to Zernike astigmatism. Most of the aberrations have derived contributions to Zernike coma. With the increase of the order of Zernike vectors, the number of aberrations that can generate effects on the Zernike vectors decrease. These qualitative relationships are helpful to understand the aberration behavior of off-axis systems.

We can find that there are the quantitative relationships between the contributions generated by the same aberration through pupil transformation, which can further describe the aberration behavior of off-axis systems. Table 2 shows the inherent relationships between the aberration contributions generated through pupil transformation for perturbed off-axis systems based on the fifth-order expansion. In Table 2, the notations ($\vec{\Psi}_{131}$, $\vec{\Psi}_{222}^2$, etc.) are applied, as defined in [30], and the difference is that the symbol "Ψ" replaces the symbol "[]." The notation $\vec{E} = \vec{L}/B$ denotes a coefficient related to the optical system parameters. $\vec{C}_{n'm'}^{Wklm}$ denotes the Fringe Zernike coefficient vector $\vec{C}_{n'm'}$ contributed from the aberration term corresponding to W_{klm} of the on-axis parent systems. Δ designates the lowest-order aperture terms, which are not discussed in this paper. These results give the corresponding vector relationships of the off-axis system with the decentered pupil center located at any position of the parent pupil (not just on the y-axis as the previous research). The inherent relationships between the derived aberrations for perturbed off-axis systems based on the partial seventh-order expansion, as examples, are listed in Table 3. The inherent relationships for other seventh-order and even higher-order derived aberrations can be obtained in the same way, and they will not be repeated here.

Tables 2 and 3 show that, in perturbed off-axis systems, the derived contributions for each aberration of the on-axis parent systems include aberrations of the same order and lower-order aperture as the original aberrations. Due to the loss of rotational symmetry, the magnitude of the derived aberration contributions is related to the magnitude and direction of the pupil decenter vector $\vec{L}$ and the corresponding misalignments.

Table 2. Inherent Vector Relationships between Derived Aberrations for Perturbed Off-Axis Systems Based on Fifth-Order Expansion

Aberration Type	Derived Aberration Contributions Generated through Pupil Transformation	Inherent Relationships between the Derived Aberration Contributions
W_{131}	$B^2\vec{L}\vec{\Psi}_{131}\cdot\vec{\rho}^2+B^3\vec{\Psi}_{131}\cdot\vec{\rho}(\vec{\rho}\cdot\vec{\rho})+\Delta$	$\vec{C}_{22}^{W131}=3\vec{E}\vec{C}_{31}^{W131}$
W_{222}	$\frac{1}{2}B^2\vec{\Psi}_{222}^2\cdot\vec{\rho}^2+\Delta$	None
W_{040}	$\begin{bmatrix}B^4W_{040}(\vec{\rho}\cdot\vec{\rho})^2+4B^3W_{040}(\vec{L}\cdot\vec{\rho})(\vec{\rho}\cdot\vec{\rho})\\+2B^2W_{040}(\vec{L}^2\cdot\vec{\rho}^2)+\Delta\end{bmatrix}$	$\begin{cases}\vec{C}_{22}^{W040}=12\vec{E}^2\vec{C}_{40}^{W040}\\\vec{C}_{31}^{W040}=8\vec{E}\vec{C}_{40}^{W040}\end{cases}$
$W_{331\mathrm{M}}$	$B^3\vec{\Psi}_{331M}\cdot\vec{\rho}(\vec{\rho}\cdot\vec{\rho})+B^2\vec{\Psi}_{331M}\vec{L}\cdot\vec{\rho}^2+\Delta$	$\vec{C}_{22}^{W331M}=3\vec{E}\vec{C}_{31}^{W331M}$
W_{422}	$\frac{1}{2}B^2\vec{\Psi}_{422}^2\cdot\vec{\rho}^2+\Delta$	None
W_{333}	$\frac{1}{4}B^3\vec{\Psi}_{333}^3\cdot\vec{\rho}^3+\frac{3}{4}B^2\vec{\Psi}_{333}^3\vec{L}^*\cdot\vec{\rho}^2+\Delta$	$\vec{C}_{22}^{W333}=3\vec{E}^*\vec{C}_{33}^{W333}$
$W_{240\mathrm{M}}$	$\begin{bmatrix}B^4\vec{\Psi}_{240M}(\vec{\rho}\cdot\vec{\rho})^2+4B^3\vec{\Psi}_{240M}(\vec{L}\cdot\vec{\rho})(\vec{\rho}\cdot\vec{\rho})\\+2B^2\vec{\Psi}_{240M}\vec{L}^2\cdot\vec{\rho}^2+\Delta\end{bmatrix}$	$\begin{cases}\vec{C}_{22}^{W240M}=12\vec{E}^2\vec{C}_{40}^{W240M}\\\vec{C}_{31}^{W240M}=8\vec{E}\vec{C}_{40}^{W240M}\end{cases}$
W_{242}	$\begin{bmatrix}\frac{1}{2}B^4(\vec{\Psi}_{242}^2\cdot\vec{\rho}^2)(\vec{\rho}\cdot\vec{\rho})+\frac{3}{2}B^2(\vec{L}\cdot\vec{L})\vec{\Psi}_{242}^2\cdot\vec{\rho}^2\\+\frac{1}{2}B^3\vec{\Psi}_{242}^2\vec{L}\cdot\vec{\rho}^3+\frac{3}{2}B^3(\vec{\Psi}_{242}^2\vec{L}^*\cdot\vec{\rho})(\vec{\rho}\cdot\vec{\rho})+\Delta\end{bmatrix}$	$\begin{cases}\vec{C}_{22}^{W242}=[3+12(\vec{E}\cdot\vec{E})]\vec{C}_{42}^{W242}\\\vec{C}_{31}^{W242}=4\vec{E}^*\vec{C}_{42}^{W242}\\\vec{C}_{33}^{W242}=4\vec{E}\vec{C}_{42}^{W242}\end{cases}$
W_{151}	$\begin{bmatrix}B^5(\vec{\Psi}_{151}\cdot\vec{\rho})(\vec{\rho}\cdot\vec{\rho})^2+B^3(\vec{\Psi}_{151}\vec{L}^2\cdot\vec{\rho}^3)\\+3B^4(\vec{\Psi}_{151}\cdot\vec{L})(\vec{\rho}\cdot\vec{\rho})(\vec{\rho}\cdot\vec{\rho})+2B^4(\vec{\Psi}_{151}\vec{L}\cdot\vec{\rho}^2)(\vec{\rho}\cdot\vec{\rho})\\+6B^3(\vec{L}\cdot\vec{L})(\vec{\Psi}_{151}\cdot\vec{\rho})(\vec{\rho}\cdot\vec{\rho})+3B^3(\vec{\Psi}_{151}^*\vec{L}^2\cdot\vec{\rho})(\vec{\rho}\cdot\vec{\rho})\\+2B^2(\vec{\Psi}_{151}\cdot\vec{L})(\vec{L}^2\cdot\vec{\rho}^2)+2B^2(\vec{L}\cdot\vec{L})(\vec{\Psi}_{151}\vec{L}\cdot\vec{\rho}^2)+\Delta\end{bmatrix}$	$\begin{cases}\vec{C}_{22}^{W151}=\begin{bmatrix}15\vec{E}\vec{C}_{51}^{W151}+20\vec{E}^2(\vec{E}\cdot\vec{C}_{51}^{W151})\\+20(\vec{E}\cdot\vec{E})\vec{E}\vec{C}_{51}^{W151}\end{bmatrix}\\\vec{C}_{40}^{W151}=5\vec{E}\cdot\vec{C}_{51}^{W151}\\\vec{C}_{33}^{W151}=10\vec{E}^2\vec{C}_{51}^{W151}\\\vec{C}_{42}^{W151}=5\vec{E}\vec{C}_{51}^{W151}\\\vec{C}_{31}^{W151}=\begin{bmatrix}4\vec{C}_{51}^{W151}+10\vec{E}^2(\vec{C}_{51}^{W151})^*\\+20(\vec{E}\cdot\vec{E})\vec{C}_{51}^{W151}\end{bmatrix}\end{cases}$
W_{060}	$\begin{bmatrix}W_{060}[B^6(\vec{\rho}\cdot\vec{\rho})^3+2B^3(\vec{L}^3\cdot\vec{\rho}^3)+6B^5(\vec{L}\cdot\vec{\rho})(\vec{\rho}\cdot\vec{\rho})^2\\+9B^4(\vec{L}\cdot\vec{L})(\vec{\rho}\cdot\vec{\rho})^2+18B^3(\vec{L}\cdot\vec{L})(\vec{L}\cdot\vec{\rho})(\vec{\rho}\cdot\vec{\rho})\\+6B^4(\vec{L}^2\cdot\vec{\rho}^2)(\vec{\rho}\cdot\vec{\rho})+6B^2(\vec{L}\cdot\vec{L})(\vec{L}^2\cdot\vec{\rho}^2)]+\Delta\end{bmatrix}$	$\begin{cases}\vec{C}_{22}^{W060}=120(\vec{E}\cdot\vec{E})\vec{E}^2\vec{C}_{60}^{W060}+90\vec{E}^2\vec{C}_{60}^{W060}\\\vec{C}_{31}^{W060}=48\vec{E}\vec{C}_{60}^{W060}+120(\vec{E}\cdot\vec{E})\vec{E}\vec{C}_{60}^{W060}\\\vec{C}_{40}^{W060}=5\vec{C}_{60}^{W060}+30(\vec{E}\cdot\vec{E})\vec{C}_{60}^{W060}\\\vec{C}_{33}^{W060}=40\vec{E}^3\vec{C}_{60}^{W060}\\\vec{C}_{42}^{W060}=30\vec{E}^2\vec{C}_{60}^{W060}\\\vec{C}_{51}^{W060}=12\vec{E}\vec{C}_{60}^{W060}\end{cases}$

Generally speaking, the derived contributions and the misalignment sensitivity of off-axis systems can be lowered by properly reducing the magnitude of the pupil decenter vector. Although each aberration generated by the same aberration of the on-axis parent systems through pupil transformation changes due to different misalignments, the quantitative relationships between these derived aberrations do not change with the misalignments. The quantitative relationships between them are the function of $\vec{E}$.

In addition, when considering a certain Zernike aberration vector, its coefficient magnitude contributed from the higher-order aperture aberrations is much larger than that contributed from the lower-order aperture aberrations. That is to say, the off-axis pupil transformation has a greater amplification effect on the higher-order aperture aberrations. Therefore, the lower-order aberrations contributed from higher-order aberrations of the on-axis parent systems through pupil transformation may be much larger than the original ones. Although the higher-order aberrations are generally small, they may have significant contributions to some low-order aberrations through amplification.

Table 3. Inherent Vector Relationships between Derived Aberrations for Perturbed Off-Axis Systems Based on Partial Seventh-Order Expansion

Aberration Type	Derived Aberration Contributions Generated through Pupil Transformation	Inherent Relationships between the Derived Aberration Contributions
$W_{531\mathrm{M}}$	$\begin{bmatrix} B^3\sum_j W_{531Mj}[(\vec{H}_{Aj}\cdot\vec{H}_{Aj})^2\vec{H}_{Aj}]\cdot\vec{\rho}(\vec{\rho}\cdot\vec{\rho}) \\ +B^2\sum_j W_{531Mj}[(\vec{H}_{Aj}\cdot\vec{H}_{Aj})^2\vec{H}_{Aj}]\vec{L}\cdot\vec{\rho}^2+\Delta \end{bmatrix}$	$\vec{C}_{22}^{W531M}=3\vec{E}\vec{C}_{31}^{W531M}$
W_{622}	$\frac{1}{2}B^2\sum_j W_{622j}[(\vec{H}_{Aj}\cdot\vec{H}_{Aj})^2\vec{H}_{Aj}^2]\cdot\vec{\rho}^2+\Delta$	None
W_{444}	$\begin{bmatrix} \frac{1}{8}B^4\sum_j W_{444j}\vec{H}_{Aj}^4\cdot\vec{\rho}^4+\frac{1}{2}B^3\sum_j W_{444j}\vec{H}_{Aj}^4\vec{L}^*\cdot\vec{\rho}^3 \\ +\frac{3}{4}B^2\sum_j W_{444j}\vec{H}_{Aj}^4(\vec{L}^2)^*\cdot\vec{\rho}^2+\Delta \end{bmatrix}$	$\begin{cases} \vec{C}_{22}^{W444}=6(\vec{E}^2)^*\vec{C}_{44}^{W444} \\ \vec{C}_{33}^{W444}=4(\vec{E})^*\vec{C}_{44}^{W444} \end{cases}$
W_{080}	$W_{080}\times$ $\begin{bmatrix} B^8(\vec{\rho}\cdot\vec{\rho})^4+8B^7(\vec{L}\cdot\vec{\rho})(\vec{\rho}\cdot\vec{\rho})^3+16B^6(\vec{L}\cdot\vec{L})(\vec{\rho}\cdot\vec{\rho})^3 \\ +12B^6(\vec{L}^2\cdot\vec{\rho}^2)(\vec{\rho}\cdot\vec{\rho})^2+48B^3(\vec{L}\cdot\vec{L})^2(\vec{L}\cdot\vec{\rho})(\vec{\rho}\cdot\vec{\rho}) \\ +36B^4(\vec{L}\cdot\vec{L})^2(\vec{\rho}\cdot\vec{\rho})^2+8B^5(\vec{L}^3\cdot\vec{\rho}^3)(\vec{\rho}\cdot\vec{\rho})+2B^4(\vec{L}^4\cdot\vec{\rho}^4) \\ +32B^4(\vec{L}\cdot\vec{L})(\vec{L}^2\cdot\vec{\rho}^2)(\vec{\rho}\cdot\vec{\rho})+48B^5(\vec{L}\cdot\vec{L})(\vec{L}\cdot\vec{\rho})(\vec{\rho}\cdot\vec{\rho})^2 \\ +8B^3(\vec{L}\cdot\vec{L})(\vec{L}^3\cdot\vec{\rho}^3)+12B^2(\vec{L}\cdot\vec{L})^2(\vec{L}^2\cdot\vec{\rho}^2)+\Delta \end{bmatrix}$	$\begin{cases} \vec{C}_{22}^{W080}=\begin{bmatrix} 504\vec{E}^2+1680(\vec{E}\cdot\vec{E})\vec{E}^2 \\ +840(\vec{E}\cdot\vec{E})^2\vec{E}^2 \end{bmatrix}\vec{C}_{80}^{W080} \\ \vec{C}_{40}^{W080}=[35+280(\vec{E}\cdot\vec{E})+420(\vec{E}\cdot\vec{E})^2]\vec{C}_{80}^{W080} \\ \vec{C}_{33}^{W080}=[448\vec{E}^3+560(\vec{E}\cdot\vec{E})\vec{E}^3]\vec{C}_{80}^{W080} \\ \vec{C}_{42}^{W080}=[280\vec{E}^2+560(\vec{E}\cdot\vec{E})\vec{E}^2]\vec{C}_{80}^{W080} \\ \vec{C}_{51}^{W080}=[96\vec{E}+336(\vec{E}\cdot\vec{E})\vec{E}]\vec{C}_{80}^{W080} \\ \vec{C}_{60}^{W080}=[7+56(\vec{E}\cdot\vec{E})]\vec{C}_{80}^{W080} \\ \vec{C}_{44}^{W080}=140\vec{E}^4\vec{C}_{80}^{W080} \\ \vec{C}_{53}^{W080}=112\vec{E}^3\vec{C}_{80}^{W080} \\ \vec{C}_{62}^{W080}=56\vec{E}^2\vec{C}_{80}^{W080} \\ \vec{C}_{71}^{W080}=16\vec{E}\vec{C}_{80}^{W080} \\ \vec{C}_{31}^{W080}=\begin{bmatrix} 224\vec{E}+1120(\vec{E}\cdot\vec{E})^2\vec{E} \\ +1344(\vec{E}\cdot\vec{E})\vec{E} \end{bmatrix}\vec{C}_{80}^{W080} \end{cases}$

3. OPTICAL ALIGNMENT STRATEGY FOR COMPLEX PERTURBED OFF-AXIS TELESCOPES BASED ON THE EXPANSION OF NODAL ABERRATION THEORY

Active optical systems can adjust the position and surface shape of optical elements through the corresponding mechanisms. When the correction type corresponds to the perturbation type, the perturbation values of optical elements need to be determined quantitatively. The previous section gives the inherent relationships between the derived aberrations for perturbed off-axis telescopes. Here, these relationships will be used to establish the active optical alignment model. When the high-order aberrations are included, the alignment model can accurately describe more complex systems and more complex surface figure errors. It can better adapt to some complex cases. The derived contributions of the third-order, fifth-order, and higher-order astigmatism with the same pupil dependence are difficult to separate from each other. For this reason, they are considered together in the alignment model. Similarly, the derived contributions of the third-order, field-cubed and higher-order coma with the same pupil dependence are also considered together. Some other aberrations can also be treated in a similar way. This section aims to give a general idea on the optical alignment of complex cases of pupil-offset off-axis telescopes. The alignment model involving fifth-order and partial higher-order aberrations, as examples, will be established in the following.

A. Alignment Model of Off-Axis Telescopes Using Nodal Aberration Theory with Fifth-Order Aberration Expansion

For perturbed off-axis telescopes, according to the relationships between the derived aberrations and the Zernike aberrations discussed in the previous section, the field dependence of some aberration contributions with the same pupil dependence can be expressed as a function of Zernike coefficient vectors, which can be given by

$$\sum_{\kappa} A\cdot\vec{\Psi}_{\kappa}=f(\ldots,\vec{C}_{22},\vec{C}_{31},\ldots,\vec{C}_{51},\ldots), \tag{11}$$

where $A\cdot\vec{\Psi}_{\kappa}$ denotes the field dependence of the aberration term considered, A denotes the corresponding conversion factor, κ is the number of the considered terms, and $f(\cdot)$ designates the function of the Fringe Zernike coefficient vectors. The specific expression will be given in the following.

In perturbed off-axis systems, to determine the contributions generated by the certain aberrations of the on-axis parent systems to the corresponding Zernike aberration, the contributions

generated by other aberrations should be subtracted from the corresponding total Zernike aberrations. Table 1 shows, that the Fringe Zernike coma ($\vec{Z}_3^1$) of perturbed off-axis systems contributes from seven parts when considering the fifth-order aberration expansion. To determine the derived contributions of the aberration terms corresponding to W_{131} and $W_{331\mathrm{M}}$ of the on-axis parent systems to Zernike coefficient vector $\vec{C}_{31}$, it is necessary to subtract the corresponding derived contributions of the third-order spherical aberration (W_{040}), a component of oblique spherical ($W_{240\mathrm{M}}$), oblique spherical (W_{242}), fifth-order field-linear coma (W_{151}), and fifth-order spherical aberration (W_{060}) from the total Zernike coefficient vector $\vec{C}_{31}$. Similarly, the Fringe Zernike coefficient vector $\vec{C}_{22}$ of perturbed off-axis systems contribute from 10 parts. To determine the derived contributions of the aberration terms corresponding to W_{222} and W_{422} to Zernike coefficient vector $\vec{C}_{22}$, the corresponding derived contributions of the third-order coma (W_{131}), third-order spherical aberration (W_{040}), field-cubed coma ($W_{331\mathrm{M}}$), trefoil (W_{333}), a component of oblique spherical ($W_{240\mathrm{M}}$), oblique spherical (W_{242}), fifth-order field-linear coma (W_{151}), and fifth-order spherical aberration (W_{060}) need to be subtracted from the total Zernike coefficient vector $\vec{C}_{22}$. In the same way, the derived contributions of other aberrations of the on-axis parent systems to the corresponding Zernike vector can also be obtained. Then, according to Tables 1 and 2, after some conversion of aberration contributions, the optical alignment model for perturbed off-axis telescopes based on NAT with fifth-order aberration expansion can be obtained, which is given by

$$\begin{cases} B^2(\vec{\Psi}_{222}^2+\vec{\Psi}_{422}^2) \\ =2(\vec{C}_{22}-\vec{M}_{31}-\vec{M}_{40}-\vec{M}_{33}-\vec{M}_{42}-\vec{M}_{51}-\vec{M}_{60}) \\ B^3(\vec{\Psi}_{131}+\vec{\Psi}_{331M})=3(\vec{C}_{31}-\vec{N}_{40}-\vec{N}_{42}-\vec{N}_{51}-\vec{N}_{60}) \\ B^3\vec{\Psi}_{333}^3=4(\vec{C}_{33}-4\vec{E}\vec{C}_{42}+10\vec{E}^2\vec{C}_{51}-40\vec{E}^3\vec{C}_{60}) \\ B^4\vec{\Psi}_{242}^2=8(\vec{C}_{42}-5\vec{E}\vec{C}_{51}+30\vec{E}^2\vec{C}_{60}) \\ B^5\vec{\Psi}_{151}=10(\vec{C}_{51}-12\vec{E}\vec{C}_{60}), \end{cases} \tag{12}$$

where

$$\begin{cases} \vec{M}_{31}=3\vec{E}\vec{C}_{31} \\ \vec{M}_{40}=-12\vec{E}^2\vec{C}_{40} \\ \vec{M}_{33}=3\vec{E}^*\vec{C}_{33} \\ \vec{M}_{42}=(3-12\vec{E}\vec{E}^*)\vec{C}_{42} \\ \vec{M}_{51}=-12\vec{E}\vec{C}_{51}+80\vec{E}^2(\vec{E}\cdot\vec{C}_{51}) \\ -10(\vec{E}\cdot\vec{E})\vec{E}\vec{C}_{51}-30\vec{E}^3(\vec{C}_{51})^* \\ \vec{M}_{60}=(60\vec{E}^2-120\vec{E}^3\vec{E}^*)\vec{C}_{60} \\ \vec{N}_{40}=8\vec{E}\vec{C}_{40} \\ \vec{N}_{42}=4\vec{E}^*\vec{C}_{42} \\ \vec{N}_{51}=4\vec{C}_{51}-40\vec{E}(\vec{E}\cdot\vec{C}_{51})+10\vec{E}^2(\vec{C}_{51})^* \\ \vec{N}_{60}=-40\vec{E}\vec{C}_{60}+120(\vec{E}\cdot\vec{E})\vec{E}\vec{C}_{60}, \end{cases} \tag{13}$$

where $\vec{C}_{n'm'}$ denotes the Fringes Zernike coefficient vector obtained by wavefront measurements. It can be seen that, in Eq. (12), the left side is the function of the aberration field decenter vectors, which can be directly related to the misalignments of optical elements.

The contribution of surface figure errors at the large aperture mirror should also be considered. If the surface with figure errors is located at the stop, the contribution can be regarded as the component of the corresponding aberrations independent of the FOV [31]. In practical engineering, the surface figure errors are generally complex, and it is difficult to describe them accurately with a single component. It is more reasonable to regard the surface figure errors as a combination of Zernike polynomial terms. If there are surface nonsymmetric figure errors at the stop, $\vec{C}_{n'm'}$ in Eq. (12) should be equal to the wavefront Zernike measurements minus the corresponding contributions of surface figure errors, which can be given by

$$\vec{C}_{n'm'}={}_{Total}\vec{C}_{n'm'}-2{}_F\vec{C}_{n'm'}, \tag{14}$$

where ${}_{Total}\vec{C}_{n'm'}$ denotes the wavefront Zernike measurements of perturbed systems, and ${}_F\vec{C}_{n'm'}$ denotes the corresponding surface Fringe Zernike figure errors. Namely, the surface figure errors are introduced into the alignment model. Therefore, the alignment model can be used to solve the misalignments and surface figure errors. If the measurement information other than wavefront measurement can be obtained, the accuracy of the alignment model can usually be improved. For example, when the boresight errors of the perturbed system can be measured, the auxiliary equations related to the aberration field decenter vectors can be obtained. This is equivalent to reducing the number of unknowns of the above model, which is beneficial to solving the alignment model. When multiple perturbations need to be determined, multiple equations need to be solved jointly. If the number of equations is more than the number of unknowns, the least-squares method can be used to determine the perturbations.

B. Alignment Model of Off-Axis Telescopes Using Nodal Aberration Theory with Higher-Order Aberration Expansion

For the approximation of third-order or fifth-order aberration expansion, the accuracy is acceptable in some simple cases of off-axis systems. However, in some complex systems, the aberration series may converge slowly. If high accuracy is desired, the contributions from higher-order aberrations should be considered [32]. In addition, if the system has complex surface figure errors, the higher-order aberrations should also be considered. Using the procedure described in Section 3.A, the alignment model for off-axis telescopes based on NAT with higher-order aberration expansion, as a relevant example, is as follows:

$$\begin{cases} B^2(\vec{\Psi}_{222}^2+\vec{\Psi}_{422}^2+\vec{\Psi}_{622}^2+\ldots) \\ =2(\vec{C}_{22}^{W222}+\vec{C}_{22}^{W422}+\vec{C}_{22}^{W622}+\ldots) \\ B^3(\vec{\Psi}_{131}+\vec{\Psi}_{331M}+\vec{\Psi}_{531M}+\ldots) \\ =3(\vec{C}_{31}^{W131}+\vec{C}_{31}^{331M}+\vec{C}_{31}^{531M}+\ldots) \\ B^3(\vec{\Psi}_{333}^3+\vec{\Psi}_{533}^3+\ldots)=4(\vec{C}_{33}^{W333}+\vec{C}_{33}^{W533}+\ldots) \\ B^4(\vec{\Psi}_{444}^4+\ldots)=8(\vec{C}_{44}^{W444}+\ldots), \end{cases} \tag{15}$$

where

$$\begin{cases} \vec{\Psi}^2_{622} = \sum\limits_j W_{622j}[(\vec{H}_{Aj}\cdot\vec{H}_{Aj})^2\vec{H}^2_{Aj}] \\ \vec{\Psi}_{531M} = \sum\limits_j W_{531Mj}[(\vec{H}_{Aj}\cdot\vec{H}_{Aj})^2\vec{H}_{Aj}] \\ \vec{\Psi}^3_{533} = \sum\limits_j W_{533j}[(\vec{H}_{Aj}\cdot\vec{H}_{Aj})\vec{H}^3_{Aj}] \\ \vec{\Psi}^4_{444} = \sum\limits_j W_{444j}\vec{H}^4_{Aj}. \end{cases} \quad (16)$$

In Eq. (15), only the expressions related to astigmatism, coma, trefoil, and tetrafoil are given. The expressions related to other aberrations can also be obtained in the same way, and they will not be repeated here. Although the higher-order aberration coefficients used in the model may be small, the accuracy of the model for some systems can be significantly improved by considering these aberrations.

It should be pointed out that the general description of the alignment model for complex cases of off-axis telescopes is given here. In specific problems, the higher-order aberration terms with less contributions to the alignment model can be ignored, which can reduce the complexity of the model and the accuracy requirement of wavefront measurements. In addition, the net aberration contributions induced by perturbations can be used in the alignment model. This can be easily obtained directly from the above model. In this way, the influence of some higher-order aberrations that are not considered in the model and are not affected by perturbations can be eliminated.

C. Solving Method of the Alignment Model Using Particle Swarm Optimization

The above alignment model is a nonlinear system of equations. When the nonlinearity of the model is strong, it is difficult to solve them accurately. The optimization method can be used to solve the nonlinear equations. The key is to construct the objective function, which is the starting point of solving the optimization problem. The alignment model in Eqs. (12) and (15) can be converted into the following form:

$$\varepsilon_\tau(X) = \sum_\kappa A_\tau\cdot\vec{\Psi}_{\tau,\kappa} - f_\tau(\vec{C}_{22}, \vec{C}_{31}, \ldots, \vec{C}_{51}, \ldots), \quad (17)$$

where $X = (X_1, X_2 \cdots X_M)^T$ denotes the decision variables (perturbation variables or their functions), M is the number of decision variables, $\varepsilon_\tau(X)$ denotes the error of the corresponding equation, $\tau = 1, 2, \cdots, \gamma$, and γ is the number of equations considered. To reduce the complexity of the alignment model, each equation in Eq. (17) can be solved separately. To determine the decision variables, overdetermined equations are often used in practical engineering. The unknowns of overdetermined equations can be obtained by solving the least square solutions. The weighted square sum of each equation in Eq. (17) at representative field points can be taken as the objective function, which is expressed as

$$\begin{cases} \min \sum\limits_{j=1}^{N} \lambda_j[\varepsilon_{\tau,j}(X)]^2, \ j = 1, 2, \cdots, N, \\ \text{s.t. } X \in D, \end{cases} \quad (18)$$

where λ_j is the field weighting factor, N is the number of representative field points, $\varepsilon_{\tau,j}(X)$ represents the error of Eq. (17) at the jth field point, and $X \in D$ denotes the decision space, which can be inequality constraints or equality constraints (if necessary), such as the equality constraints related to boresight errors. The number of inequality and equality constraints can be none or many, depending on the specific application. The feasible region will be a multi-dimensional space satisfying bounds on variables, inequality, and equality constraints. In Eq. (17), the equation with the surface figure errors of Zernike higher-order aperture is solved first because of fewer unknowns. The higher-order aperture figure errors can be obtained, and then they are substituted into other equations to be solved sequentially. The equation with the surface figure errors of lowest-order aperture is finally solved. Thus, the problem of solving nonlinear equations is transformed into the optimization problem.

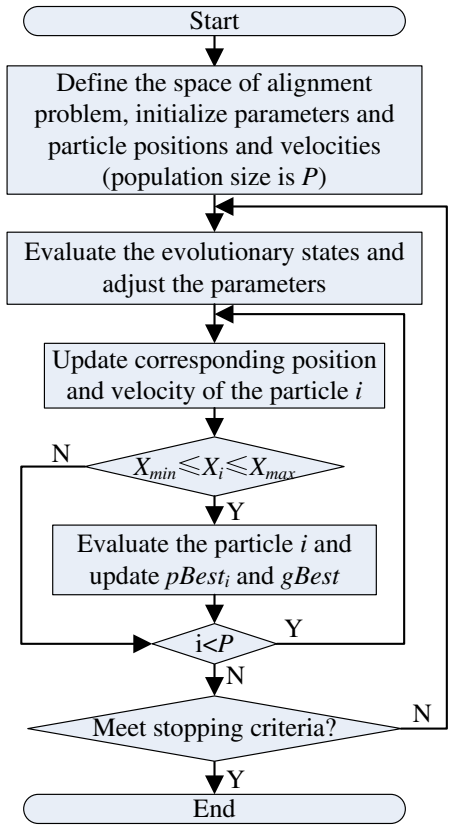

Fig. 2. Flow chart of PSO algorithm for the alignment model.

Here, the particle swarm optimization algorithm (PSO) [33] is utilized to solve the alignment model. PSO is a general optimization method, which has the advantages of good global search ability, fast calculation speed, and less parameters to be adjusted; thus, it is becoming increasingly utilized in the field of function optimization. The flow chart of the PSO algorithm for the alignment problem is shown in Fig. 2. The procedure of the algorithm for the alignment problem is described as follows:

Step 1: Define the space of alignment problem and initialize parameters.

Step 2: Initialize the particle positions and velocities (population size is P). These particle positions represent the set of alignment solutions, which are the aberration field decenter vectors and the surface figure errors of optical elements.

Step 3: Evaluate the evolutionary states and adjust the parameters.

Step 4: Update the position X_i and velocity V_i of the corresponding particle. The range of particle position is $[X_{\min}, X_{\max}]$.

Step 5: Evaluate the associated particle state and update the individual particle best ($pBest_i$) and global optimal position ($gBest$).

Step 6: Repeat Steps 3–5 until the terminal condition is satisfied, and present the results.

The decision variables of the above alignment model of perturbed off-axis systems can be determined by using the steps mentioned above. Of course, if the accuracy requirement of the decision variables is not high, the alignment model can be simplified and solved analytically.

4. VERIFICATION OF SYSTEM ALIGNMENT OF THE PERTURBED OFF-AXIS THREE-MIRROR ANASTIGMATIC TELESCOPE WITH MISALIGNMENTS AND COMPLEX SURFACE FIGURE ERRORS BASED ON THE PROPOSED METHOD

A. Alignment Example

To verify the effectiveness and accuracy of the approach proposed above, in this section, a system alignment is demonstrated. As an example of complex perturbed off-axis systems, the off-axis TMA telescope with misalignments and complex surface figure errors is considered. Most large optical telescopes have the aperture stop located on PM. So here, the stop is located on PM, which is chosen as the coordinate reference. The aberration field decenter vectors of SM and TM can be expressed as

$$\begin{cases} \vec{\sigma}_{\mathrm{SM}}^{sph} = (\vec{S} + c_{\mathrm{SM}}\vec{T})/G_M, \\ \vec{\sigma}_{\mathrm{SM}}^{asph} = \vec{T}/G_P, \\ \vec{\sigma}_{\mathrm{TM}}^{sph} = \vec{P} + 2(1 + c_{\mathrm{TM}}d_2)[(1 + c_{\mathrm{SM}}d_1)\bar{u}_{\mathrm{PM}}]\vec{\sigma}_{\mathrm{SM}}^{sph}/G_S, \\ \vec{\sigma}_{\mathrm{TM}}^{asph} = \vec{Q} + 2d_2(1 + c_{\mathrm{SM}}d_1)\bar{u}_{\mathrm{PM}}\vec{\sigma}_{\mathrm{SM}}^{sph}/G_A, \end{cases} \tag{19}$$

where

$$\begin{cases} \vec{S} = \begin{bmatrix} \mathrm{BDE}_{\mathrm{SM}} \\ -\mathrm{ADE}_{\mathrm{SM}} \end{bmatrix}, \vec{T} = -\begin{bmatrix} \mathrm{XDE}_{\mathrm{SM}} \\ \mathrm{YDE}_{\mathrm{SM}} \end{bmatrix}, \\ \vec{P} = \frac{c_{\mathrm{TM}}}{G_S}\begin{bmatrix} \mathrm{XDE}_{\mathrm{TM}} \\ \mathrm{YDE}_{\mathrm{TM}} \end{bmatrix} + \frac{1}{G_S}\begin{bmatrix} -\mathrm{BDE}_{\mathrm{TM}} \\ \mathrm{ADE}_{\mathrm{TM}} \end{bmatrix}, \vec{Q} = \frac{1}{G_A}\begin{bmatrix} \mathrm{XDE}_{\mathrm{TM}} \\ \mathrm{YDE}_{\mathrm{TM}} \end{bmatrix}, \\ G_M = (1 + c_{\mathrm{SM}}d_1)\bar{u}_{\mathrm{PM}}, \\ G_P = d_1\bar{u}_{\mathrm{PM}}, \\ G_S = [c_{\mathrm{TM}}(d_2 - d_1) + 2c_{\mathrm{SM}}(c_{\mathrm{TM}}d_1d_2 + d_1) + 1]\bar{u}_{\mathrm{PM}}, \\ G_A = [d_2 + d_1(2c_{\mathrm{SM}}d_2 - 1)]\bar{u}_{\mathrm{PM}}, \end{cases} \tag{20}$$

where $\vec{\sigma}_{\mathrm{TM}}^{sph}$ and $\vec{\sigma}_{\mathrm{TM}}^{asph}$ designate the aberration field decenter vectors for TM; $\vec{\sigma}_{\mathrm{SM}}^{sph}$ and $\vec{\sigma}_{\mathrm{SM}}^{asph}$ denote the aberration field decenter vectors for SM; $\mathrm{XDE}_{\mathrm{TM}}$, $\mathrm{YDE}_{\mathrm{TM}}$, $\mathrm{ADE}_{\mathrm{TM}}$, and $\mathrm{BDE}_{\mathrm{TM}}$ denote the misalignments of TM; $\mathrm{XDE}_{\mathrm{SM}}$, $\mathrm{YDE}_{\mathrm{SM}}$, $\mathrm{ADE}_{\mathrm{SM}}$, and $\mathrm{BDE}_{\mathrm{SM}}$ are the misalignments of SM; c_{TM} denotes the curvature of TM. c_{SM} is the curvature of SM, $\bar{u}_{\mathrm{PM}}$ is the incidence angle of the chief ray at the primary mirror, d_1 is the mirror spacing between PM and SM, d_2 is the spacing between SM and TM, and the superscript sph and asph denote contributions of the spherical base and aspheric departure, respectively. For the spherical base, the relevant optical characteristic point is the location of the center of curvature of the surface.

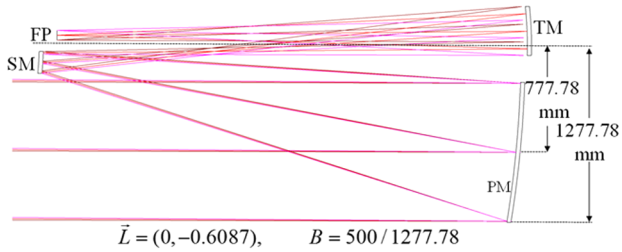

Fig. 3. Optical layout of the off-axis TMA telescope.

Table 4. Introduced Figure Errors (I-V) and Computed Figure Errors (C-V)[a]

	${}_F C_5^{\mathrm{PM}}$	${}_F C_6^{\mathrm{PM}}$	${}_F C_{10}^{\mathrm{PM}}$	${}_F C_{11}^{\mathrm{PM}}$	${}_F C_{17}^{\mathrm{PM}}$	${}_F C_{18}^{\mathrm{PM}}$
I-V	0.0600	−0.0500	−0.0600	0.0400	−0.0400	0.0500
C-V	0.0595	−0.0496	−0.0596	0.0403	−0.0398	0.0502

[a] ${}_F C_i^{\mathrm{PM}}$ denotes the surface figure errors. The Fringe Zernike coefficients are in λ.

Here, both misalignments and complex surface figure errors are considered. The perturbation values can be determined in two steps. The first step is to solve the surface figure errors and the aberration field decenter vectors. They can be obtained by solving the Eq. (17). The second step is to determine the misalignments of SM and TM, which can be obtained by solving the Eq. (19).

The optical layout of the off-axis TMA telescope used in this paper is shown in Fig. 3. It has a stop aperture diameter of 1000 mm with a 2.3° × 0.3° FOV. The radius values of PM, SM, and TM are −8004.06, −2021.03, and −2712.44, respectively. The conic values of PM, SM, and TM are −0.921, −4.717, and −0.293, respectively. The thickness values between mirrors are −3446.93 and 3491.15, respectively. To perform this example, several FOVs were selected, which were (1.15°, −0.15°), (−1.15°, −0.15°), (−1.15°, −0.45°), (1.15°, −0.45°), (0°, −0.3°), (0.58°, −0.15°), (0.58°, −0.45°), (−0.58°, −0.15°), and (−0.58°, −0.45°), respectively. It is assumed that the figure errors of PM were complex, including the components of Zernike astigmatism $\vec{Z}_2^2$ (i.e., Fringe Zernike terms Z_5 and Z_6), trefoil $\vec{Z}_3^3$ (i.e., Z_{10} and Z_{11}), and tetrafoil $\vec{Z}_4^4$ (i.e., Z_{17} and Z_{18}). The introduced misalignments were the misalignments of SM and TM. The search space of the aberration field decenter vectors was (−1, 1). The search space of the surface figure errors was (−0.5, 0.5). The population size of PSO was 40. The maximum number of iterations of PSO was 2000. By using the proposed method, the perturbation values of the off-axis TMA telescope can be obtained. The introduced and computed figure errors are presented in Table 4. The introduced and computed misalignments of SM are listed in Table 5. The introduced and computed misalignments of TM are presented in Table 6.

Table 5. Introduced Misalignments (I-M) and Computed Misalignments (C-M) of SM[a]

	XDE_{SM}	YDE_{SM}	ADE_{SM}	BDE_{SM}
I-M	0.1500	−0.1500	−0.0150	0.0150
C-M	0.1489	−0.1513	−0.0151	0.0149

[a]XDE and YDE are in mm. ADE and BDE are in degrees.

Table 6. Introduced Misalignments (I-M) and Computed Misalignments (C-M) of TM[a]

	XDE_{TM}	YDE_{TM}	ADE_{TM}	BDE_{TM}
I-M	−0.2500	0.2500	0.0200	−0.0200
C-M	−0.2478	0.2473	0.0197	−0.0202

[a]XDE and YDE are in mm. ADE and BDE are in degrees.

As can be seen in Tables 4–6, the introduced and computed results are nearly the same magnitude, showing that the method proposed above is very effective. The accuracy of the lateral TM misalignments was lower than that of the lateral SM misalignments. The reason may be that SM is more sensitive to the wave aberration of the off-axis TMA telescope than TM. Therefore, the accuracy of the lateral SM misalignments is more easily guaranteed. To correct the perturbed off-axis telescope, the negative values of the computed misalignments and surface figure errors were introduced into the perturbed system in the optical simulation software. The full field displays (FFDs) before and after correction for coupling paired Fringe Zernike coefficient terms are show in Fig. 4. As can be seen, after the system is corrected based on the proposed method, the typical aberration fields can be nearly restored to nominal states. Although only the figure errors on the primary mirror were considered in this section, the

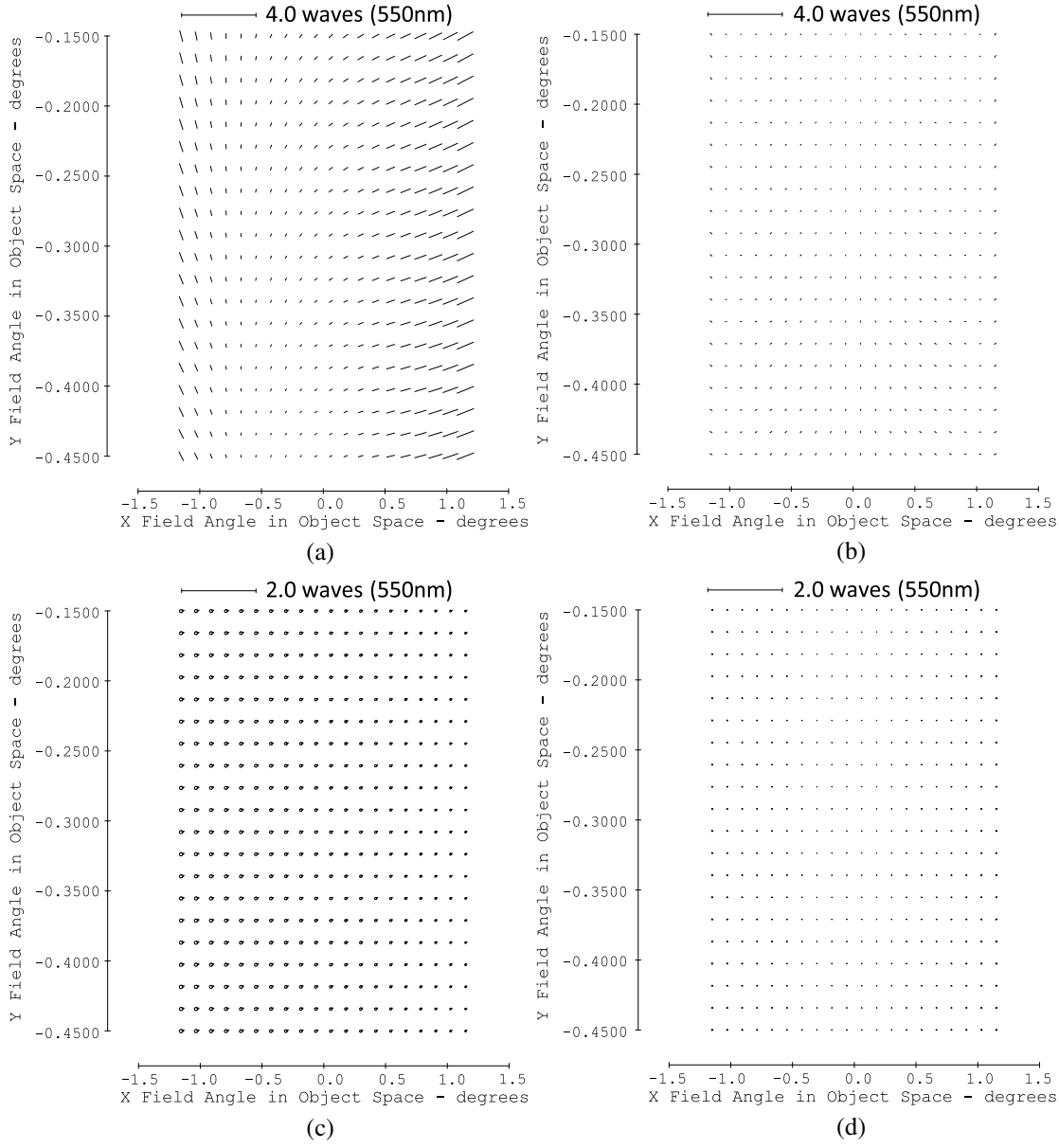

Fig. 4. Full-field displays (FFDs). (a) FFDs (anamorphic scaling) for Z5/Z6 before correction, which includes the contributions from mirror figure errors and misalignments. (b) FFDs for Z5/Z6 after correction. (c) FFDs for Z7/Z8 before correction. (d) FFDs for Z7/Z8 after correction.

Table 7. Four Different Cases Considered in Monte Carlo Simulations[a]

	XDE, YDE	ADE, BDE	${}_F C_i^{\mathrm{PM}}$	M-E
Case 1	[−0.05, 0.05]	[−0.005, 0.005]	[−0.02, 0.02]	\
Case 2	[−0.5, 0.5]	[−0.02, 0.02]	[−0.05, 0.05]	\
Case 3	[−1.5, 1.5]	[−0.05, 0.05]	[−0.1, 0.1]	\
Case 4	[−0.5, 0.5]	[−0.02, 0.02]	[−0.05, 0.05]	3%

[a]XDE and YDE are in mm, ADE and BDE are in degrees, the Fringe Zernike coefficients are in λ, and M-E denotes the measurement errors, $i = 5, 6, 10, 11, 17, 18$.

method could be extended to take into account the figure errors on the surface away from the stop through the specific pupil footprint for each field point.

B. Monte Carlo Simulation

To further demonstrate the correctness and accuracy of the method proposed in this paper, the Monte Carlo simulation was performed for the off-axis TMA telescope. Four different cases were adopted in the process, which are shown in Table 7. In Case 1, Case 2, and Case 3, the perturbation ranges increase in sequence without measurement errors. In Case 4, it has the same perturbation ranges as Case 2, but with 3% relative measurement errors for the corresponding Fringe Zernike coefficients.

In the simulation, 100 trial perturbation states were randomly generated following a uniform distribution for each case. There are 400 pairs of perturbations for all cases. Then, the simulation for each trial system could be performed by using the proposed method and the ST method.

The root mean square deviations (RMSDs) were used for each case to evaluate the accuracy, which are given by

$$\mathrm{RMSD}_j = \sqrt{\frac{1}{100}\sum_{n=1}^{100}[X_j(n) - x_j(n)]^2}, \tag{21}$$

where $X_j(n)$ and $x_j(n)$ represent the introduced and computed values for the jth perturbation, respectively. The RMSD results of perturbations for each case using the proposed method and the ST method are shown in Fig. 5.

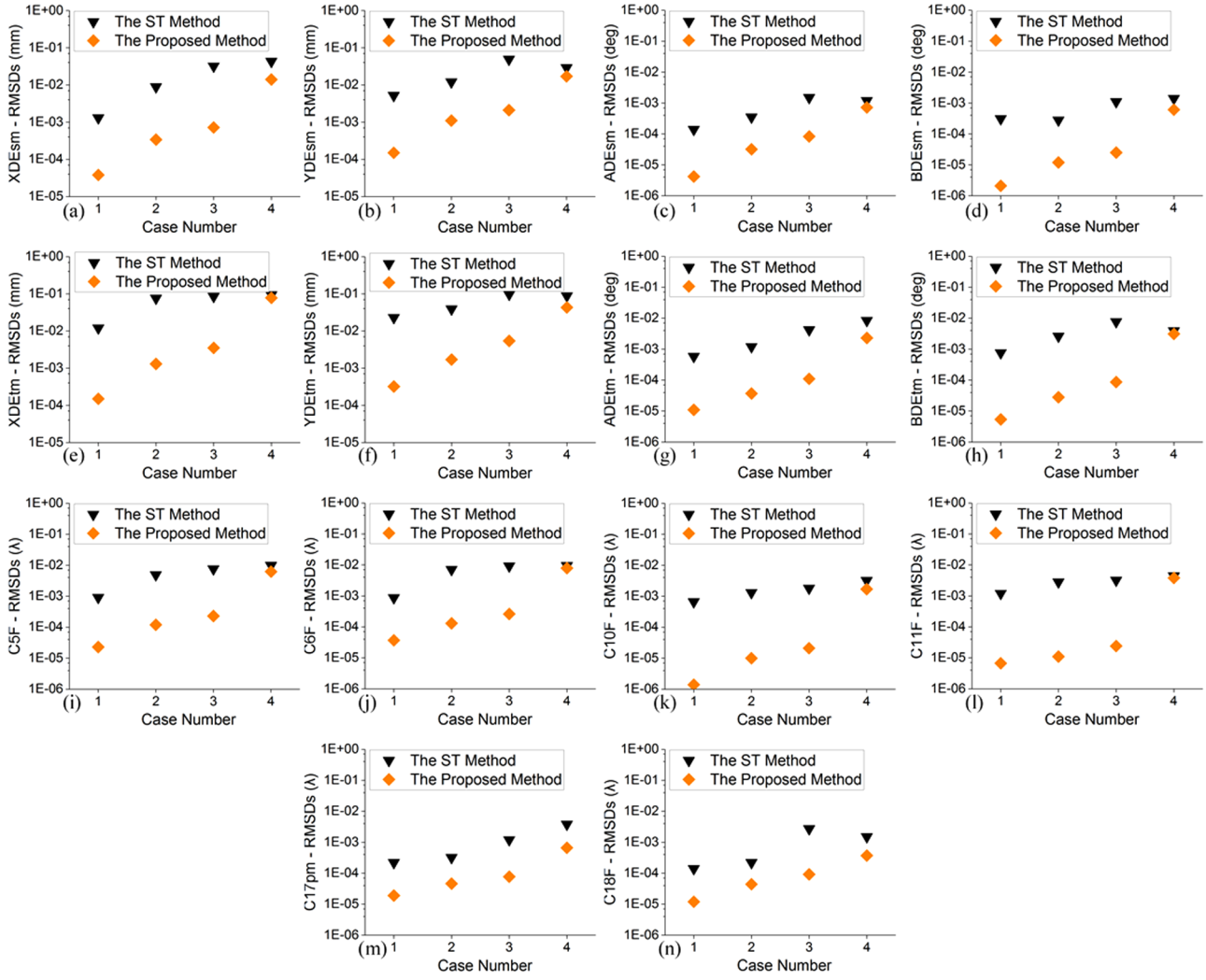

Fig. 5. RMSDs using the proposed method and the ST method for different cases. (a)–(d) for misalignments of SM, (e)–(h) for misalignments of TM, and (i)–(n) for surface figure errors. The triangular marks denote the RMSDs using the ST method. The square marks denote the RMSDs using the proposed method.

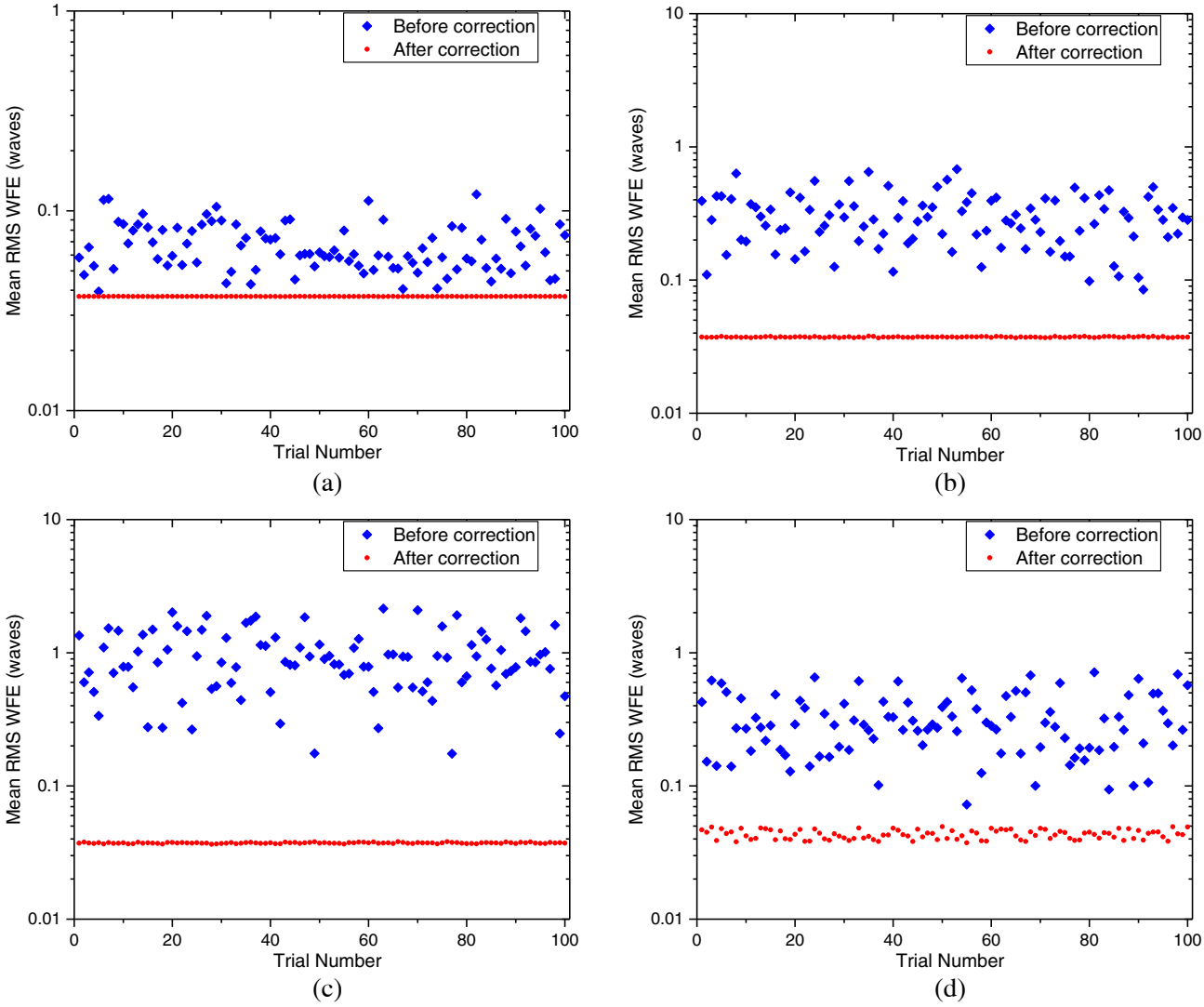

Fig. 6. System WFEs (average RMS) before and after correction for four cases using proposed method. (a) WFEs for Case 1, (b) Case 2, (c) Case 3, and (d) Case 4. The square marks denote system WFEs before correction. The dot marks denote system WFEs after correction.

As in Fig. 5, the results for Cases 1–3 demonstrate the correctness and accuracy of the method proposed in this paper. In contrast, the proposed method is more accurate than the ST method. The ST method is limited by the nonlinear relationships between the measurement values and perturbation parameters. As the perturbation ranges increase, the calculated perturbation values using the ST method may be inaccurate. A comparison of the results for Case 4 show the proposed method is also affected by the measurement errors. Even so, the proposed method is more accurate than the ST method at the considered level of measurement errors. To overcome the uncertainty of measurement errors, it is suggested that more measurements at different azimuthal FOVs are carried out.

To evaluate the results more fully, the average RMS WFEs were given for each trial system with equally spaced field points in $2.3° \times 0.3°$. The system WFEs (average RMS) before and after correction using the proposed method are shown in Fig. 6. The system WFEs before and after correction using ST method are shown in Fig. 7. As can be seen in Figs. 6 and 7, the trial optical systems in Case 1 can be nearly aligned to the nominal state based on two methods. In Cases 2 and 3, the system WFEs after correction based on the ST method are bigger in most conditions. Namely, as the perturbation ranges increase, the average RMS WFEs based on the ST method become significantly larger. The ST method is suitable for small range perturbations because of the nonlinear sensitivity. However, the accuracy of the proposed method is almost unaffected by the perturbation ranges. In Case 4, as measurement errors are considered, the average RMS WFEs based on both methods become larger. Even so, the proposed method is also more reliable than the ST method. The results show that the method proposed in this paper is a better choice for alignment of the off-axis telescope.

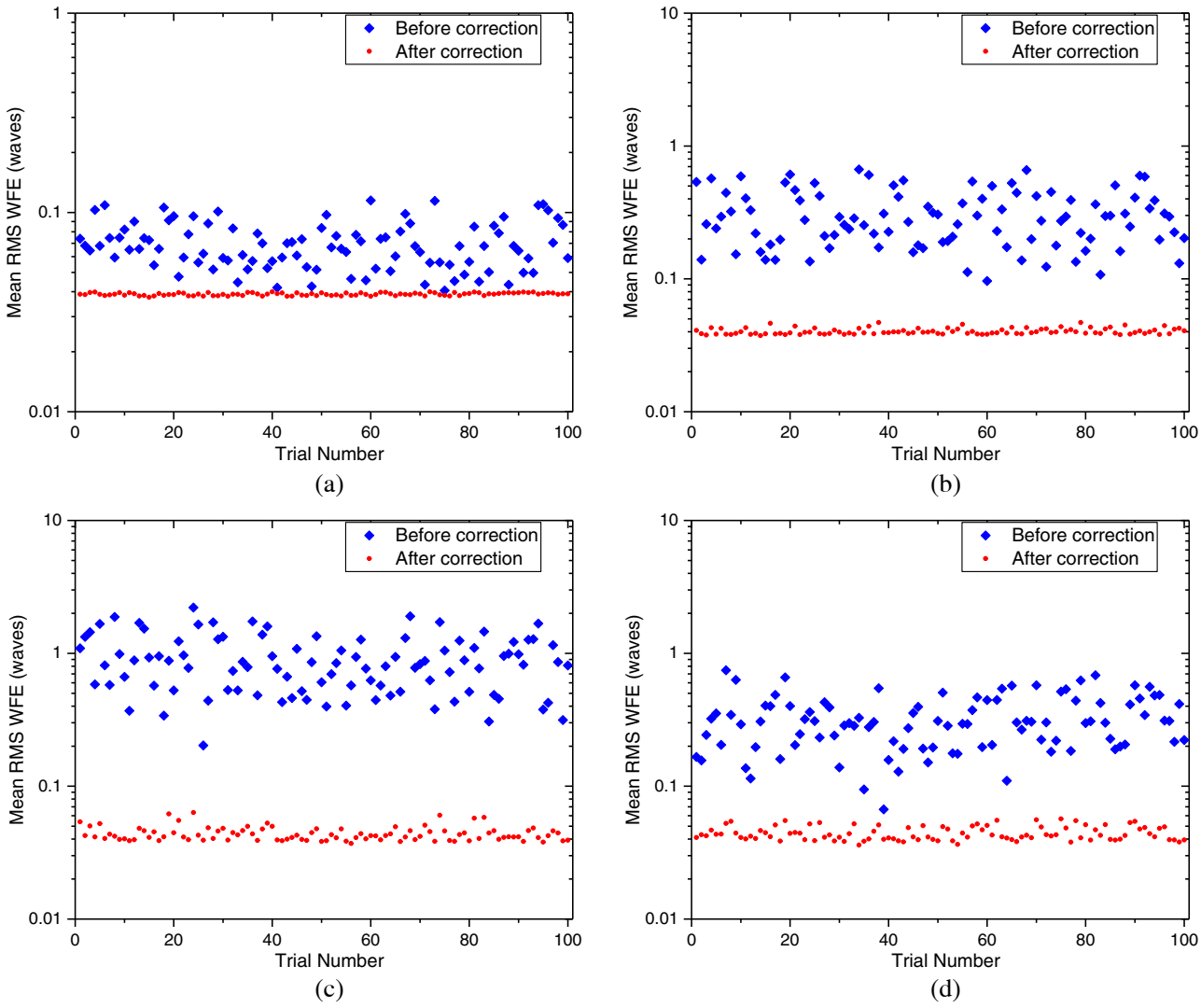

Fig. 7. System WFEs (average RMS) before and after correction for four cases using the ST method. (a) WFEs for Case 1, (b) Case 2, (c) Case 3, and (d) Case 4. The square marks denote system WFEs before correction. The dot marks denote system WFEs after correction.

5. CONCLUSION

This paper aimed to give a general idea of optical alignment using NAT for complex perturbed pupil-offset off-axis telescopes. The direct vector expansion of the wave aberration function for perturbed off-axis systems was given, which can conveniently convert the corresponding higher-order terms into the existing aberration types. The inherent vector relationships between the contributions generated by the aberrations of the on-axis parent systems through pupil transformation were obtained, which are helpful to understand the aberration behavior of off-axis systems. According to the inherent vector relationships, the analytical alignment model based on NAT for complex cases of perturbed off-axis telescopes was established. It can quantitatively separate the effects of misalignments and surface figure errors from the total aberration fields. By taking the weighted square sum of each function in the alignment model as the objective function, the nonlinear alignment model was solved by particle swarm optimization algorithm. Then the off-axis TMA telescope with misalignments and complex figure errors (including Zernike astigmatism, trefoil, and tetrafoil) was taken as an example, and the system alignment results were given. The misalignments and complex surface figure errors can be determined accurately. After correction, the system aberration fields were nearly restored to the nominal states. Monte Carlo simulations were carried out and demonstrated the correctness and accuracy of the proposed method. The proposed alignment method can well adapt to the case of perturbed pupil-offset off-axis telescopes. As long as the off-axis telescopes can be accurately characterized by NAT, they can be well aligned based on the idea proposed in this paper. This work can provide a helpful reference for optical alignment and analysis of complex perturbed off-axis systems.

Funding. National Natural Science Foundation of China (61705223, 61905241); ShuGuang Talents Scheme Award of Changchun Institute of Optics, Fine Mechanics and Physics, Chinese Academy of Sciences; National Key Research and Development Program of China (2016YFB0500100).

Disclosures. The authors declare no conflicts of interest.

Data Availability. Data underlying the results presented in this paper are not publicly available at this time but may be obtained from the authors upon reasonable request.

REFERENCES

1. R. N. Wilson, "Active optics and the New Technology Telescope (NTT): the key to improved optical quality at lower cost in large astronomical telescopes," Contemp. Phys. **32**, 157–171 (1991).
2. R. N. Wilson, F. Franza, and L. Noethe, "Active optics: I. A system for optimizing the optical quality and reducing the costs of large telescopes," J. Mod. Opt. **34**, 485–509 (1987).
3. N. Devaney, C. Reinlein, N. Lange, M. Goy, A. Goncharov, and P. Hallibert, "HYPATIA and STOIC: an active optics system for a large space telescope," Proc. SPIE **9904**, 990469 (2016).
4. F. Kenny, N. Devaney, A. Goncharov, M. Goy, and C. Reinlein, "An active optics system for large UVOIR space telescopes," Proc. SPIE **10698**, 106986C (2018).
5. N. Devaney, F. Kenny, A. Goncharov, M. Goy, and C. Reinlein, "Development of a prototype active optics system for future space telescopes," Appl. Opt. **57**, E101–E106 (2018).
6. L. G. Cook, "Three-mirror anastigmat used off-axis in aperture and field," Proc. SPIE **183**, 207–211 (1979).
7. H. J. Juranek, R. Sand, J. Schweizer, B. Harnisch, B. Kunkel, E. Schmidt, A. Litzelmann, F. Schillke, and G. Dempewolf, "Off-axis telescopes: the future generation of Earth observation telescopes," Proc. SPIE **3439**, 104–115 (1998).
8. R. Upton, T. Rimmele, and R. Hubbard, "Active optical alignment of the Advanced Technology Solar Telescope," Proc. SPIE **6271**, 62710R (2006).
9. S. Kim, H. S. Yang, Y. W. Lee, and S. W. Kim, "Merit function regression method for efficient alignment control of two-mirror optical systems," Opt. Express **15**, 5059–5068 (2007).
10. R. V. Shack and K. P. Thompson, "Influence of alignment errors of a telescope system," Proc. SPIE **251**, 146–153 (1980).
11. K. Thompson, "Description of the third-order optical aberrations of near-circular pupil optical systems without symmetry," J. Opt. Soc. Am. A **22**, 1389–1401 (2005).
12. K. P. Thompson, "Multinodal fifth-order optical aberrations of optical systems without rotational symmetry: spherical aberration," J. Opt. Soc. Am. A **26**, 1090–1100 (2009).
13. K. P. Thompson, "Multinodal fifth-order optical aberrations of optical systems without rotational symmetry: the comatic aberrations," J. Opt. Soc. Am. A **27**, 1490–1504 (2010).
14. K. P. Thompson, "Multinodal fifth-order optical aberrations of optical systems without rotational symmetry: the astigmatic aberrations," J. Opt. Soc. Am. A **28**, 821–836 (2011).
15. K. P. Thompson, T. Schmid, O. Cakmakci, and J. P. Rolland, "Real-ray-based method for locating individual surface aberration field centers in imaging optical systems without rotational symmetry," J. Opt. Soc. Am. A **26**, 1503–1517 (2009).
16. G. Ju, C. Yan, Z. Gu, and H. Ma, "Aberration fields of off-axis two mirror astronomical telescopes induced by lateral misalignments," Opt. Express **24**, 24665–24703 (2016).
17. G. Ju, C. Yan, Z. Gu, and H. Ma, "Nonrotationally symmetric aberrations of off-axis two-mirror astronomical telescopes induced by axial misalignments," Appl. Opt. **57**, 1399–1409 (2018).
18. X. Bai, B. Xu, B. Ma, Y. Gao, S. Xu, and G. Ju, "Aberration fields of pupil-offset off-axis two-mirror astronomical telescopes induced by ROC error," Opt. Express **28**, 30447–30465 (2020).
19. G. Ju, H. Ma, and C. Yan, "Aberration fields of off-axis astronomical telescopes induced by rotational misalignments," Opt. Express **26**, 24816–24834 (2018).
20. X. Zhang, S. Xu, H. Ma, and N. Liu, "Optical compensation for the perturbed three mirror anastigmatic telescope based on nodal aberration theory," Opt. Express **25**, 12867–12883 (2017).
21. X. Zhang, D. Zhang, S. Xu, and H. Ma, "Active optical alignment of off-axis telescopes based on nodal aberration theory," Opt. Express **24**, 26392–26413 (2016).
22. Z. Gu, C. Yan, and Y. Wang, "Alignment of a three-mirror anastigmatic telescope using nodal aberration theory," Opt. Express **23**, 25182–25201 (2015).
23. G. Ju, C. Yan, Z. Gu, and H. Ma, "Computation of astigmatic and trefoil figure errors and misalignments for two-mirror telescopes using nodal-aberration theory," Appl. Opt. **55**, 3373–3386 (2016).
24. J. Sebag, W. Gressler, T. Schmid, J. P. Rolland, and K. P. Thompson, "LSST telescope alignment plan based on nodal aberration theory," Publ. Astron. Soc. Pac. **124**, 380–390 (2012).
25. J. Wang, B. Guo, Q. Sun, and Z. Lu, "Third-order aberration fields of pupil decentered optical systems," Opt. Express **20**, 11652–11658 (2012).
26. H. Hu, J. Liu, and Z. Fan, "Interaction of pupil offset and fifth-order nodal aberration field properties in rotationally symmetric telescopes," Opt. Express **21**, 17986–17998 (2013).
27. R. A. Buchroeder, "Tilted component optical systems," Ph.D. dissertation (University of Arizona, 1976).
28. J. C. Wyant and K. Creath, "Basic wavefront aberration theory for optical metrology," in *Applied Optics and Optical Engineering*, R. R. Shannon and J. C. Wyant, eds. (Academic, 1992), pp. 1–53.
29. R. W. Gray and J. P. Rolland, "Wavefront aberration function in terms of R. V. Shack's vector product and Zernike polynomial vectors," J. Opt. Soc. Am. A **32**, 1836–1847 (2015).
30. K. P. Thompson, K. Fuerschbach, and J. P. Rolland, "An analytic expression for the field dependence of FRINGE Zernike polynomial coefficients in optical systems that are rotationally nonsymmetric," Proc. SPIE **7849**, 784906 (2010).
31. T. Schmid, J. P. Rolland, A. Rakich, and K. P. Thompson, "Separation of the effects of astigmatic figure error from misalignments using Nodal Aberration Theory (NAT)," Opt. Express **18**, 17433–17447 (2010).
32. K. Fuerschbach, J. P. Rolland, and K. P. Thompson, "Theory of aberration fields for general optical systems with freeform surfaces," Opt. Express **22**, 26585–26606 (2014).
33. Z. H. Zhan, J. Zhang, Y. Li, and H. S. Chung, "Adaptive particle swarm optimization," IEEE Trans. Syst. Man. Cybern. **39**, 1362–1381 (2009).